PROCEEDINGS OF ISAP '92, SAPPORO, JAPAN

Analysis of Circularly Polarized Stacked Microstrip Antenna

T.M.Au, The Chinese U. of Hong Kong, Shatin, N.T., Hong Kong
K.M.Luk, City Polytechnic of Hong Kong, Kowloon, Hong Kong
K.F.Lee, U. of Toledo, Toledo, OH, USA

ABSTRACT

The variations of the input impedance, impedance bandwidth, axial ratio bandwidth and far field radiation patterns of a stacked rectangular microstrip antenna with the position of the parasitic element are investigated theoretically. The moment method and Galerkin procedure are employed to solve for the solutions. It is found that the characteristics vary significantly with the position of the parasitic patch. The results are compared with experimental data available in the literature.

INTRODUCTION

In recent years, the circular polarization characteristics of microstrip antenna are extensively investigated. The development of Mobile Satellite (MSAT) communication and Earth remote sensing using microstrip antenna are reported on [1]. To overcome the narrow impedance bandwidth of microstrip antenna, the single patch element is constructed on physically thick or high dielectric substrate [2]. Moreover, the two layer electromagnetically coupled (EMCP) antenna with airgap has better impedance bandwidth, axial ratio bandwidth and directivity [3-4].

In this paper, the input impedance, impedance bandwidth, axial ratio bandwidth and far field radiation patterns of a stacked rectangular microstrip antenna are investigated by the methods of moments. The unknown surface patch current densities are formulated in the spectral domain and are decomposed into n entire basis functions with unknown amplitudes. Galerkin procedure is employed to solve for the solutions. The formulation can be considered as a generalization of the methods by Pozar [5]. The theoretical results are compared with measurements [3].

THEORY

The geometry of the structure to be considered is shown in Figure 1. An idealized excitation current $\vec{J}_i = \delta(x-x_p)\,\delta(y-y_p)\,\hat{z}$ feeding the lower patch at $(x,y,z)=(x_p,y_p,l)$ is assumed. The lower patch on $z=l$ and upper (parasitic) patch on $z=l+s+h$ are supported by dielectric layers of relative permittivity ε_r. An air-gap of thickness s separates the two dielectric layers.

The first step of the analysis is to derive the electric fields (Green's functions) of point horizontal electric current elements located on the lower and upper substrate surfaces. Specifically current I_1 and I_2 directed to the positive x-axis and located respectively at (x_{01},y_{01},l) and $(x_{02},y_{02},l+s+h)$ are considered. The electric field produced by individual current is obtained by considering the Fourier transforms [8] of the field components in separate regions and matching the tangential components at the interfaces subjecting to boundary conditions.

Results for the Fourier transforms of the components of the magnetic vector potential $\vec{A}(x,y,z)$ produced by the current elements in different regions are expressed in [6]. The electric field components are then derived from the magentic vector potential.

According to the boundary conditions, the tangential electric field on the metal patch is zero, which is produced by the excitation current $\vec{J}_i$ and the surface current densities $\vec{J}_{s1}$ on the lower patch at $z=l$, and $\vec{J}_{s2}$ on the parasitic patch at $z=l+s+h$. The formulated integral equation is formulated as follows:

$$\vec{E}(\vec{J}_{s1})+\vec{E}(\vec{J}_{s2})+\vec{E}(\vec{J}_i) = 0 \quad \begin{matrix} \text{at } z=l,\ 0<x<2a_1,\ 0<y<2w_1 \\ \text{and} \\ \text{at } z=l+s+h,\ 0<x<2a_2,\ 0<y<2w_2 \end{matrix} \tag{1}$$

The unknown surface current densities on the patches are expanded into a sets of n basis functions:

$$\vec{J}_{si} = \sum_{m=1}^{N_i} I_{mi}^{x} J_{mi}^{x}\,\hat{x} + \sum_{n=1}^{N_{i+2}} I_{ni}^{y} J_{ni}^{y}\,\hat{y} \qquad , i=1,2 \tag{2}$$

where $I_{ni}^{x,y}$ is the unknown amplitude of the basis function $J_{ni}^{x,y}$. Next, equations (3) and (4) are substituted into equation (1) which are then weighted with the testing functions identical to the basis functions. The matrix equation is expressed as:

$$\underset{N_t\times N_t}{[Z]}\ \underset{N_t\times 1}{[I]} = \underset{N_t\times 1}{[V]} \qquad , N_t = \sum_{i=1}^{4} N_i \tag{3}$$

Technique for evaluating each impedance element in equation (3) can be referred to [5]. Method of folding around the pole is employed to minimize the error in finding the pole location of the Green function.

The input impedance Z_{in} of the microstrip antenna can be obtained from a variational formula:

$$Z_{in} = -\sum_{i=1}^{2}\left[\sum_{m=1}^{N_i} I_{mi}^{x} V_{mi}^{x} + \sum_{n=1}^{N_{i+2}} I_{ni}^{y} V_{ni}^{y}\right] \tag{4}$$

Regarding the basis functions, Entire Basis (EB) modes are chosen in this analysis. Equation (2) is in the following form:

$$\vec{J}_{si}(x,y) = \begin{cases} \sum_{m=1}^{N_i} \dfrac{I_{mi}^{x}}{2w_i}\sin\left(\dfrac{m\pi}{2a_i}x\right)\hat{x} + \sum_{n=1}^{N_{i+2}} \dfrac{I_{ni}^{y}}{2a_i}\sin\left(\dfrac{n\pi}{2w_i}y\right)\hat{y} & 0<x<2a_i \text{ and } 0<y<2w_i,\ i=1,2 \\ 0 & \text{elsewhere} \end{cases} \tag{5}$$

where a_i and w_i $(i=1,2)$ are the dimensions of the patches (Figure 1).

ILLUSTRATIVE RESULTS

In this section, the numerical results are obtained to compare with experimental data available in the literature. The dimensions of a rectangular microstrip antenna with parasitic element are as follows: $a_1=a_2=22.25\text{mm}$, $w_1=w_2=22.0\text{mm}$, $l=h=0.25\text{mm}$, $\varepsilon_r=2.17$ and the location (x_0,y_0) of coaxial feed is (10.6mm,10.5mm).

Figure 2 shows the convergence behaviour of the input impedance of the stacked antenna with $s=15.3\text{mm}$. It is found that the resistance of the input impedance converges to the steady solution as $n\geq 5$ but the reactance of the input impedance converges slowly when increasing the number of expansion modes. In this analysis, we choose $N_1=N_2=N_3=N_4=5$ to calculate the theoretical value of input impedance with different space s between two dielectric layers.

Figure 3 shows the theoretical value of far field radiation patterns of the single layer patch antenna compared with measurement [3]. Note that E_ϕ^{yz} and E_θ^{xz} represent E_ϕ in $y-z$ plane and E_θ in $x-z$ plane, and E_ϕ^{xz} and E_θ^{yz} represent E_ϕ in $x-z$ plane and E_θ in $y-z$ plane. Moreover, the resonant frequency, impedance bandwidth, axial ratio bandwidth and resonant resistance are 2.352 GHz, 0.234%, 0.208% and 19.44Ω, respectively.

Figure 4 shows the far field radiation patterns of stacked antenna compared with $s=0.0$ mm and measurement [3]. It is found that the measured data is closed to the theoretical values of E_ϕ^{xz} and E_ϕ^{yz} for ϕ smaller than 30°.

Figure 5 shows the far field radiation patterns of stacked antenna with $s=88.9$ mm compared with measurement [3]. It is found that the beamwidth is narrower than the previous cases.

Figure 6 shows the impedance bandwidth of stacked antenna versus different substrate spacing in term of resonant wavelength λ_0 of single patch case. The impedance bandwidth is determined by VSWR<2. It is found that the maximum bandwidth is 1.9296 at $s = 0.10\lambda_0$.

Figure 7 shows the axial ratio bandwidth of stacked antenna versus different substrate spacing in term of resonant wavelength λ_0 of single patch case. It is found that the peak value of %ARBW is 0.503% at $s = 0.11\lambda_0$. As s is increased, the calculated value of ARBW is approximate same for the number of expansion mode is set to one or five.

Figure 8 shows the resonant resistance of stacked antenna with different substrate spacing in term of resonant wavelength λ_0 of single patch. The resonant resistance is determined by $E_\phi^{yz} = E_\phi^{xz}$. It is found that the resonant resistance is increased as %ARBW increased. The maximum value of the resonant resistance is 43.61Ω at $0.12\lambda_0$.

CONCLUSION

In this paper, full-wave analysis is employed to evaluate the characteristics of circularly polarizated of the stacked microstrip antenna. It is found that the parasitic element can increase the antenna impedance, impedance bandwidth, axial ratio bandwidth and changes the far field radiation pattern for properly spacing s.

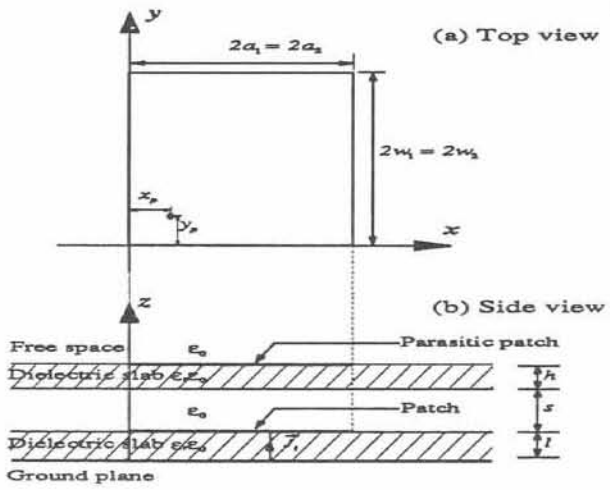

Fig. 1 Geometry of the stacked antenna. (a) Top view. (b) Side view.

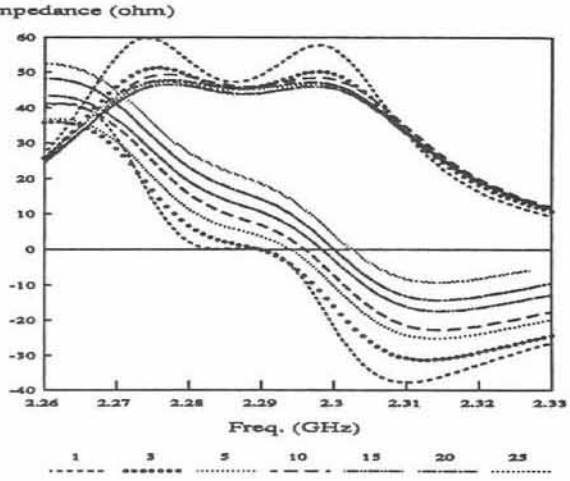

Fig. 2 The convergence behaviour of input impedance of stacked antenna with $s = 15.3$ mm.

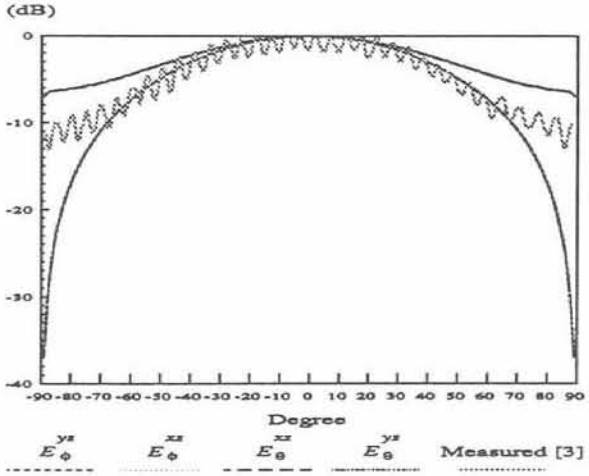

Fig. 3. Far field radiation patterns of a single layer patch antenna.

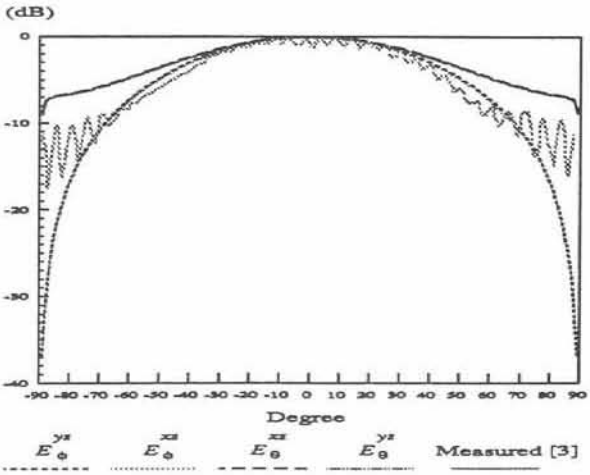

Fig. 4. Far field radiation patterns of stacked antenna with $s = 0.0$ mm.

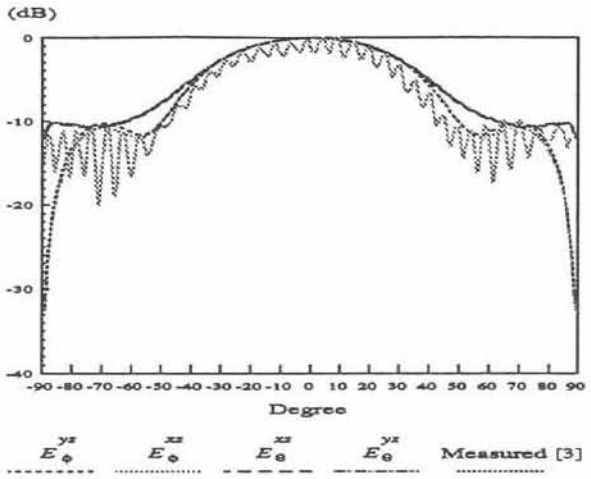

Fig. 5. Far field radiation patterns of stacked antenna with $s = 88.9$ mm.

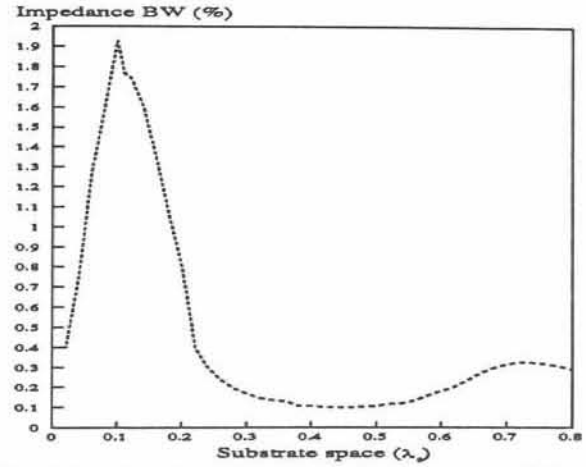

Fig. 6. Impedance bandwith of satcked antenna versus different substrate space in term of resonat wavelength λ_0 of single patch.

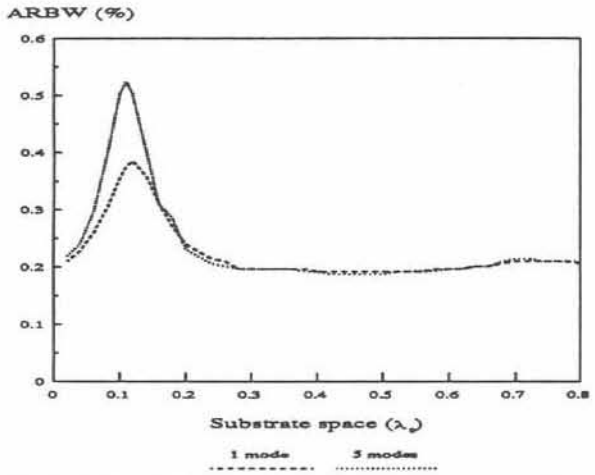

Fig. 7. Axial ratio bandwidth of stacked antenna versus different substrate spacing in term of resonant wavelength λ_0 of single patch.

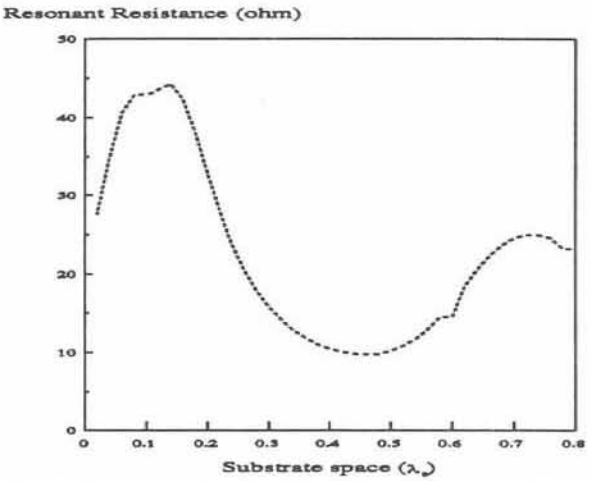

Fig. 8. Resonant resistance of stacked antenna versus different substrate spacing in term of resonant wavelength λ_0 of single patch.

REFERENCES

[1] J.Huang, "Recent microstrip antenna development at JPL", *Progress In Electromagnetic Research Symposium,* pp.282, 1991.

[2] R.C.Hall, J.R.Mosig, "The analysis of feed pin effects in wide-band circularly polarization patch antennas", *ibid,* pp.283, 1991.

[3] R.Q.Lee, T.Talty and K.F.Lee, "Circular polarization characteristics of stacked microstrip antenna", *Electron.Lett.*, pp.2109-2110, 1990.

[4] R.Q.Lee, K.F.Lee and Z.Fan, "Some recent analysis of microstrip antenna with parasitic elements", *Progress In Electromagnetic Research Symposium,* pp.603, 1991.

[5] D.M.POZAR, "Input impedance and mutual coupling of rectangular microstrip antennas", *IEEE Trans. Antenna Propagat.*, vol 30, pp.1191-1196, 1982.

[6] T.M.Au and K.M.Luk, "Effect of parasitic element on the characteristics of microstrip antenna", vol 39, *ibid,* pp.1247-1251, 1991.